Proceedings of FEDSM2002
2002 ASME Fluids Engineering Division Summer Meeting
July 14-18, 2002, Montreal, Quebec, Canada

FEDSM2002-

ENTRAINMENT CORRELATIONS BASED ON A FUEL/WATER STRATIFIED SHEAR FLOW

Peter A. Chang, III*
Wesley Wilson
Paisan Atsavapranee
Hydromechanics Directorate
Naval Surface Warfare Center — Carderock Division
West Bethesda, Maryland 20817-5700
Email: changpa@nswccd.navy.mil

Xiongjun Wu
Joseph Katz
Department of Mechanical Engineering
The Johns Hopkins University
Baltimore, Maryland 21218
Email: katz@titan.me.jhu.edu

ABSTRACT

The purpose of this work was twofold: first, to develop correlations for the entrainment of small fuel droplets into water in a stratified fuel/water shear flow; second, to implement the correlations in a CFD code and validate it with experimental effluent fuel concentration data. It is assumed that the droplets act as passive scalars and are advected far from their generation regions where they may cause fuel contamination problems far downstream. This work relied upon extensive experimental data obtained from a stably stratified shear flow: droplet number, droplet PDF, fluid fraction and velocity field data. The droplet data was expressed as a nondimensional entrainment velocity (E) for the volume flux of fuel due to small droplets. The fluid fraction and velocity fields at the interface were expressed in terms of Richardson numbers (Ri). It was found that $E = C_e Ri^{-n}$ where $n = 1$ and C_e is a constant, gives a good fit for the two experimental velocity cases. The best correlation was implemented in a computational simulation of the stably stratified shear flow, and the results show that the simulation can predict the entrainment quite well. A second simulation was performed for a flow with energetic vertical buoyant jets ("buoyant flow events") and stably stratified shear flows with very large Richardson numbers. In this case, the simulations underpredicted effluent fuel concentrations by two orders of magnitude. *Ad hoc* corrections to the entrainment correlations show marked improvements.

INTRODUCTION

The accuracy of effluent fuel concentration predictions for immiscible stably stratified two-fluid systems depends primarily upon the validity of the entrainment rate of droplets at the liquid-liquid interface. Once entrained, droplets, if small enough, will be advected by the continuous phase liquid. In the case of the refueling of ship's compensated fuel/ballast tanks (CFBTs), in which water ("compensating water") is displaced by diesel fuel, diesel fuel droplets in the compensating water are an environmental concern if discharged overboard. See Chang *et al.* (2001) for more information regarding CFBT hydrodynamics. While many references exist for the entrainment of miscible liquids (*e.g.*, Fernando, 1991 and Atsavapranee and Gharib, 1997) few such references exist for immiscible flows.

Wu and Katz (1999, 2000, 2001) have performed experiments on a stably stratified shear flow with diesel fuel and water, characterizing the flows and obtaining droplet and velocity field data. The present study uses these experimental data to develop correlations between the velocity fields and the entrainment rate of fuel droplets at a stably stratified fuel/water interface. It is assumed that effluent fuel concentrations consist only of small droplets and therefore entrainment correlations are developed using just the fraction of droplets below a certain size. The advantage of this approach is that the buoyancy forces on the droplets can be neglected, and the number of droplets can be expressed as a single scalar, the Small Droplet Concentration (SDC). In this paper, the development of the experimental correlations and

*Address all correspondence to this author.

their implementation in a computational fluid dynamics code are shown in detail. Results of simulations on the shear flow and a three-bay model of a CFBT are shown. Comparison to experimental results are quite good.

DEVELOPMENT OF DROPLET ENTRAINMENT MODEL

An SDC advection equation, applicable to shear flow experimental droplet data, is now derived. Consider a water-filled control volume bounded at the top by the fuel/water interface. If it is assumed that the flow is primarily in the streamwise direction, the lateral advection through the sides and the vertical advection through the bottom can be neglected. An advection equation for the SDC is

$$\frac{\partial \phi}{\partial t} + \frac{\partial u\phi}{\partial x} = \frac{w_e A_z}{\Delta V}. \tag{1}$$

ϕ is the SDC, u is the streamwise velocity and A_z is the interface area. w_e is the entrainment velocity which represents the flux of entrained fuel per unit interface area. The shear flow experiment was conducted in a steady state mode, so it can be further assumed that the droplet statistical properties are invariant in time so that $\frac{\partial \phi}{\partial t} \rightarrow 0$. Also it is assumed that the change in ϕ is much greater than the change in u, and that ϕ is small. Then (1) becomes

$$U_c \frac{\partial \phi}{\partial x} = \frac{w_e A_z}{\Delta V} \tag{2}$$

where U_c is a droplet convection velocity. Let Φ' be the Small Droplet Volume (SDV), the volume occupied by only the small droplets in the shear flow test subvolume, ΔV_o be test subvolume and A_{zo} be the test interface area, so that $\Phi' = \Delta V_o \phi$. Then (2) becomes,

$$\frac{w_e}{U_c} = \frac{1}{A_{zo}} \frac{\partial \Phi'}{\partial x.} \tag{3}$$

The shear flow droplet data has been used to evaluate the right-hand-side of (3) (denoted by E_{rhs}). The left-hand-side is denoted by E $(E \equiv w_e/U_c)$.

Derivation of Entrainment Rate

E_{rhs} was determined from the droplet probability density functions (PDFs) and droplet number data from the stably stratified shear flow experiments. A schematic of the experiment is shown in Figure 1. Silhouette photography was used to visualize the fuel/water interface and droplets and particle image velocimetry (PIV) techniques to capture the velocity fields and turbulence quantities in the water layer. The mean water velocity was $0.8\ m/sec$ and $1.2\ m/sec$ with a small fuel velocity, sufficient to replace the fuel entrained in the water layer. For more details see Wu and Katz (1999, 2000, 2001). Let $p(d_i;x,\ell)$ be the droplet size PDF for droplet diameter d_i, at location x, in layer ℓ; $ell = 1,2,3$ for the fuel, mixed, and water layers, respectively (Figure 2). The mixed layer consists of a high concentration of droplets, most of which are fuel droplets. The PDF is defined by

$$p(d_i) = \frac{h_i}{\sum_{i=1}^{B} h_i} \tag{4}$$

where h_i is the number of droplets in size bin d_i and B is the number of bins. The cumulative fraction of droplets for which $d_i \leq d_j$ is given by

$$c(d_j) = \sum_{i=1}^{j} p\,(d_i;x,\ell)\,. \tag{5}$$

$d_j = 1.5\ mm$ was chosen for this study which is a compromise between the need to characterize only the smallest droplets and the need to use enough data such that the resulting functions are smooth enough to curve fit. The smallest droplets resolved in the experiment were $0.75\ mm$ in diameter. Let $N'(x;r)$ denote the total number of droplets of all sizes for the test section interface area, $A_{zo} = \Delta x \Delta y$, where $\Delta x = 5\ cm$ is the length of the data window, and $\Delta y \approx 2\ cm$ is the depth of field. When $c(d_j)$ is weighted by the droplet volumes, and then multiplied by $N'(x;r)$, the volume of droplets for $0 < d \leq d_j$ is obtained:

$$\Phi'(x;\ell,d \leq d_j) = N'(x;\ell) \left[\sum_{i=1}^{j} p(d_i;x,\ell) \frac{\pi}{6} d_i^3. \right] \tag{6}$$

If the x-derivative of (6) is normalized by A_{zo}, the non-dimensional entrainment rate, E_{rhs}, is obtained,

$$\begin{aligned} E_{rhs} &= \frac{1}{A_{zo}} \frac{\partial}{\partial x} \Phi'(x;\ell,d \leq d_j) \\ &= \frac{1}{A_{zo}} \frac{\partial}{\partial x} \left\{ N'(x;\ell) \left[\sum_{i=1}^{j} p(d_i;x,\ell) \frac{\pi}{6} d_i^3 \right] \right\} \end{aligned} \tag{7}$$

We are primarily concerned with droplets that have been ejected into the water layer. The PDFs for all layers is based on the order of 10^3 droplets per x-location, while PDFs for the water layer are based on approximately $1/10$ the number of droplets. Thus, the cumulative fractions for the smallest bins (5) were not smooth enough to determine any trends in Φ' for the water layer. The results shown here are based on the PDFs for all layers. Figure 3 is an example of $p(d;x,\ell)$, for all layers for $1.2\ m/sec$.

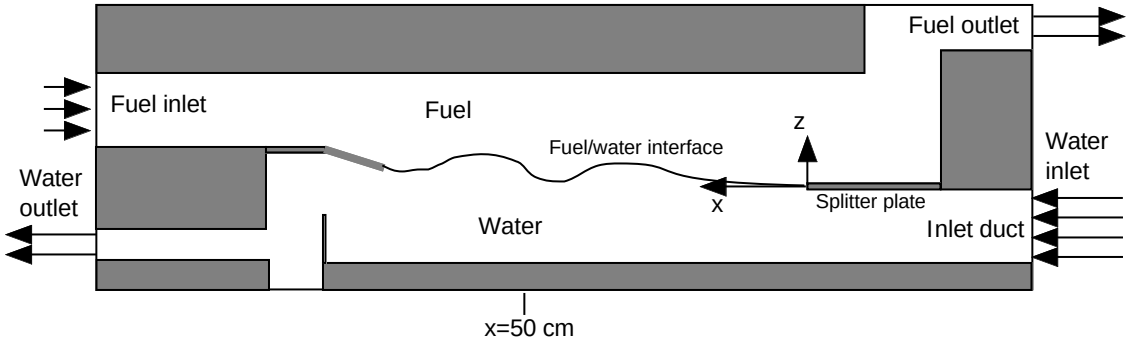

Figure 1. SHEAR FLOW GEOMETRY.

The proportion of smaller droplets decreases with x. These observations are consistent with the notion that the higher levels of energy exerted on the interface in the upstream locations produce proportionally more small droplets. Another, related, explanation might be that upstream droplet generation mechanisms occur over shorter length scales, whereas further downstream the droplets have been generated over larger length scales as might occur with the Kelvin-Helmholtz (K-H) rollup processes. The comparison shows that the data for all layers are much smoother than for the water layer.

Figure 4 shows the number of droplets, $N'(x;\ell)$, for the three layers individually, as well as the total summed over the three layers for the 1.2 m/sec velocity case. Note that in Figure 4 N' for the fuel and water layers have different vertical scales for clarity. The number of droplets in the water layer remains constant up to about $x = 30\ cm$ with an increase in the slope as x increases further. The number of droplets in the mixture layer increases with a relatively constant slope, except between $x = 15 - 20\ cm$, where it has a slightly steeper slope.

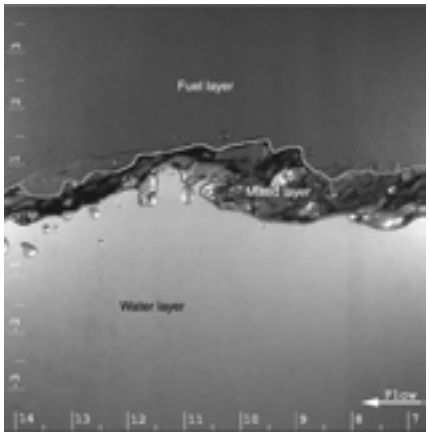

Figure 2. PHOTOGRAPH SHOWING DEFINITION OF SHEAR FLOW LAYERS.

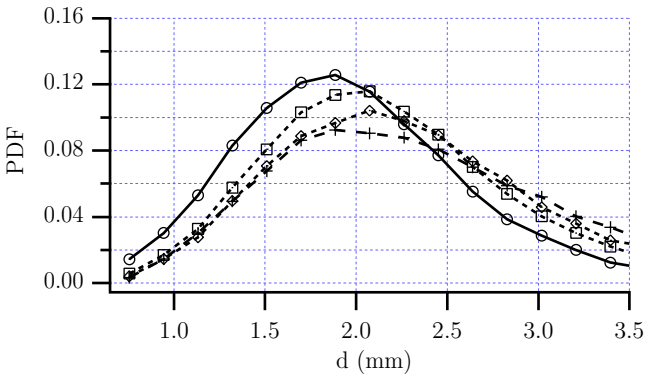

Figure 3. DROPLET SIZE PDFS *vs.* DIAMETER FOR ALL LAYERS; 1.2 m/sec; $\circ$: $x = 5\ cm$; $\square$: $x = 15\ cm$; $\diamond$: $x = 25\ cm$; $+$: $x = 35\ cm$.

Figure 5 shows $\Phi'(x;\ell, d \leq 1.5\ mm)$ computed using (6) for all layers. Both velocity cases undergo sharp increases in the same x-ranges. Figure 6 shows $d\Phi'/dx$ for all layers. The data for all layers is heavily weighted by the droplets in the mixture layer and for our purposes should reflect the mixture layer behavior. The data for 1.2 m/sec shows that the flux is initially very small, rising quickly to a peak at $x = 15\ cm$. It then decreases, in general, as x increases.

Correlations between Flow Field Data and Entrainment Rate

It is well known that the entrainment of one fluid into another at a fluid-fluid interface is dependent upon the balance of inertial, buoyancy, and possibly surface tension forces. The inertial forces create the shear stresses that lead to interface deformations and eventual breakdown into droplets. The buoyancy and surface tension forces tend to damp the formation of interface deformations. The Richardson number is the ratio of the buoyancy to inertial forces, so a smaller value of the Richardson number

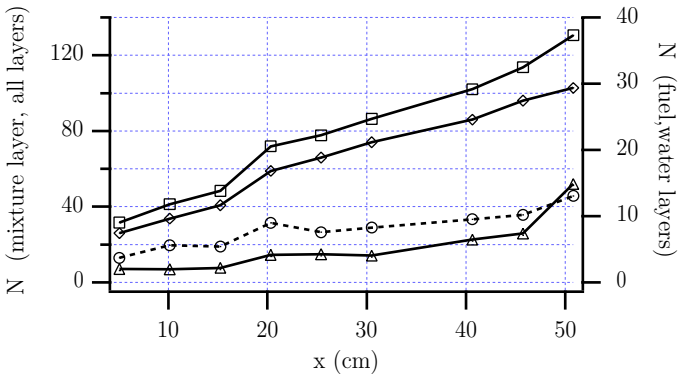

Figure 4. NUMBER OF DROPLETS, N', *vs.* x FOR $1.2\,m/sec$; $\triangle$: WATER LAYER, $\diamond$: MIXTURE LAYER, $\circ$: FUEL LAYER, $\square$: ALL LAYERS.

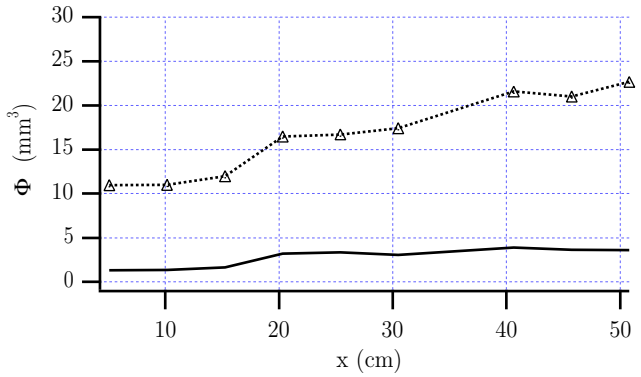

Figure 5. SMALL DROPLET VOLUMES, Φ', *vs.* x FOR ALL LAYERS; ——— : $0.8\,m/sec$; $\triangle$: $1.2\,m/sec$.

indicates a greater inclination for entrainment.

The entrainment is typically nondimensionalized as in (3). For miscible flows Fernando (1991) shows that

$$\frac{w_e}{U_{ch}} = C_e Ri^{-n} \tag{8}$$

where C_e and n are constants and U_{ch} is a characteristic velocity. Typically, $0.5 \leq n \leq 1.5$ and for counterflows, $n = 1$.

Three forms of the Richardson number were studied. The shear Richardson number, Ri_s, is defined as

$$Ri_s = \frac{\Delta B}{U_\infty S}. \tag{9}$$

$\Delta B = g(\rho_w - \rho_f)/\rho_f$ where g is the acceleration of gravity and ρ_f and ρ_w are the densities of fuel and water, respectively; U_∞

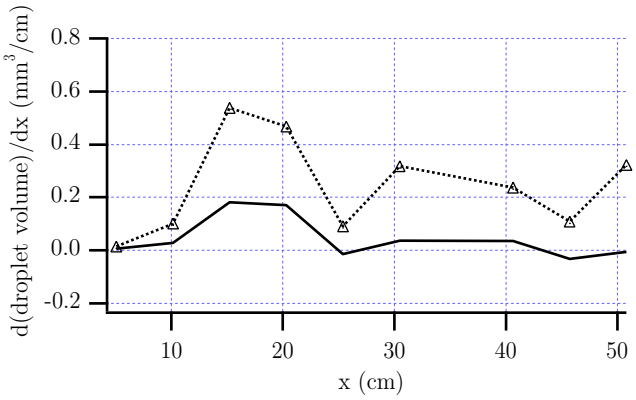

Figure 6. DERIVATIVE OF SDV, $(\frac{\partial \Phi'}{\partial x})$, *vs.* x FOR ALL LAYERS; ——— : $0.8\,m/sec$; $\triangle$: $1.2\,m/sec$.

is the difference between the upper and lower mean flow velocities in the shear flow facility and S is the velocity shear rate at the interface based on time-averaged velocity and interface location data. Ri_α is the fuel volume fraction gradient Richardson number,

$$Ri_\alpha = \frac{\Delta B \frac{\partial r}{\partial z}}{S^2} \tag{10}$$

where $\frac{\partial r}{\partial z}$ is the fuel volume fraction gradient computed from values at the edge of the mixed layer. The mixture layer Richardson number is

$$Ri_h = \frac{\Delta B}{\delta_m S^2} \tag{11}$$

where δ_m is the mixture layer thickness [$\delta_m = z(r = 0.99) - z(r = 0.01)$].

Wu and Katz (2001) showed that Ri_s increases monotonically, flattening out at high x-values. On the other hand, Ri_α (Figure 7) and Ri_h dip down at low-x values, and then increase, but not monotonically. From a computational standpoint, Ri_s would be difficult to implement because for arbitrary flow situations the choice of U_∞ is not clear. Ri_α and Ri_h, on the other hand, rely only on data at the interface, and thus, in theory, do not suffer from this ambiguity.

In order to find a function of the Richardson number that fits the data various values of the exponent n in (8) were applied to the Richardson number data. The shape of the resulting curves, plotted *vs.* x, were compared with the entrainment data shown in Figure 6. It was determined that $n = 1$, when applied to the Ri_α and Ri_h curves, gave a shape closest to the entrainment data. The constants C_e were then determined such that the Ri_α^{-n} and Ri_h^{-n}

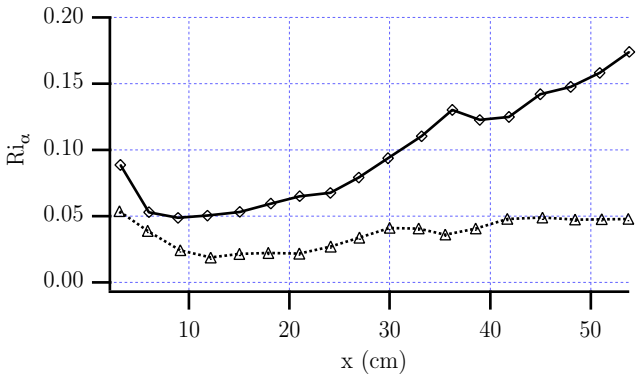

Figure 7. EXPERIMENTAL VALUES OF Ri_α FROM WU AND KATZ (2001): $\triangle$: 0.8 m/sec; $\diamond$: 1.2 m/sec.

functions would match the entrainment data. Interestingly, for each of the functions, a single constant gave relatively close fits for *both* velocity cases, indicating strongly that the relationship has some universality.

Figures 8 and 9 shows E_{rhs} compared with two proposed Richardson number correlations

$$g_\alpha = C_{e\alpha} Ri_\alpha^{-n} = 1.0 \times 10^{-6} Ri_\alpha^{-1} \tag{12}$$

$$g_h = C_{eh} Ri_h^{-n} = 1.8 \times 10^{-6} Ri_h^{-1} \tag{13}$$

Both the Richardson number correlations mimic the sharp increase in generation rate for $x < 15\ cm$ followed by the gradual decrease at larger values of x. While both capture the essence of the curve, Ri_α comes closest to capturing the correct location of the peak at $x = 15\ cm$. Also, both velocity cases compare well using a single constant of proportionality.

In the simulations, the entrainment velocity is computed by

$$w_e = U_c g_\alpha \tag{14}$$

where Ri_α is computed at the fuel/water interface (vertical index k). The convection velocity is the horizontal velocity magnitude at the interface:

$$U_c = \left(u_k^2 + v_k^2\right)^{1/2}. \tag{15}$$

and SDC injected into the flow is

$$\Delta\phi = \frac{w_e A_z \Delta t}{\Delta V}. \tag{16}$$

Δt is the time step size and ΔV is the subvolume.

The constants $C_{e\alpha}$ and C_{eh} in (12) and (13), respectively, are much smaller than those shown in Fernando (1991) for a miscible counterflow:

$$\frac{w_e}{U_\infty} = 8 \times 10^{-4} Ri_u^{-1} \tag{17}$$

where

$$Ri_u \equiv \frac{g\Delta\rho\delta_m}{\rho U_\infty^2}. \tag{18}$$

One reason for the discrepancy may be that for a miscible flow the entrainment rate includes *all* the entrained fluid, whereas in an immiscible flow, the smallest droplets can be separated out, as was done here, and comprise only a small proportion of the total entrained fluid. Furthermore, the surface tension, not included in this study, probably plays a role when extending these results to other liquid-liquid systems.

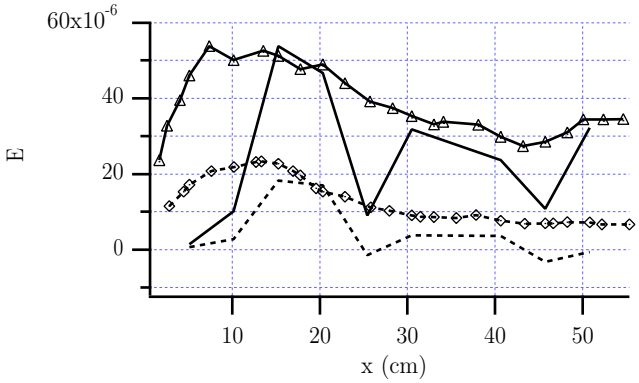

Figure 8. ENTRAINMENT RATES COMPARED WITH Ri_h CORRELATION, EQN. (13); ——— : $E(0.8\ m/sec)$; - - - - - - - - : $E(1.2\ m/sec)$; $\triangle$: $g(Ri_h)$ FOR 0.8 m/sec; ..... : $g(Ri_h)$ FOR 1.2 m/sec.

COMPUTATIONAL IMPLEMENTATION

The entrainment correlation (12) was implemented into the *FLOW-3D*[1] viscous flow solver and run on the shear flow and a three-bay model. *FLOW-3D* versions 7.5 and 7.7 were used for the shear flow and version 8.0 for the three-bay model. The two-fluid option was used to simulate the fuel and water flows. This

[1] *FLOW-3D* is a registered trademark of FlowScience, Inc., Santa Fe, NM.

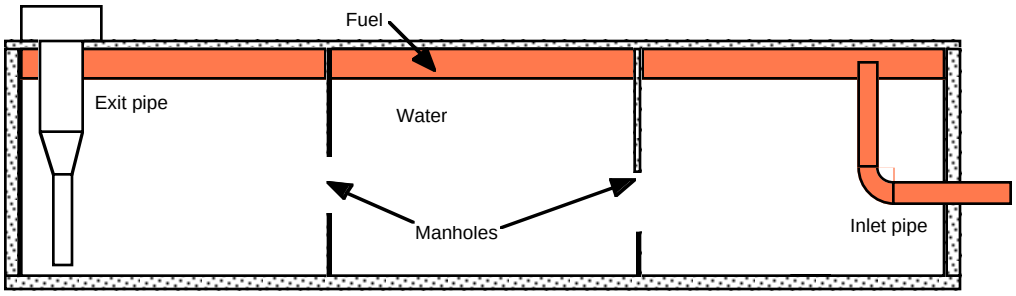

Figure 10. SKETCH OF THE THREE-BAY MODEL AND INITIAL FLUID CONFIGURATION.

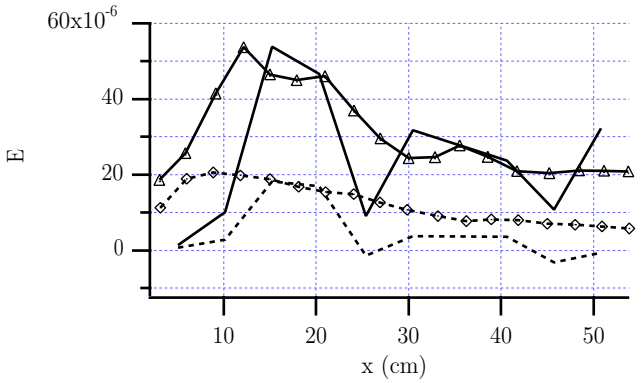

Figure 9. ENTRAINMENT RATES COMPARED WITH FUNCTION OF Ri_α CORRELATION, EQN. (12); ——— : $E(0.8\ m/sec)$; - - - - - - - - : $E(1.2\ m/sec)$; △ : $g(Ri_\alpha)$ FOR $0.8\ m/sec$; ..... : $g(Ri_\alpha)$ FOR $1.2\ m/sec$.

solves a single set of mass, momentum and turbulence equations with variable density and viscosity. An advection equation which uses a Volume of Fluid advection algorithm was used to track the fuel volume fraction, r. A drift flux approximation was used to model the relative motions of fuel and water in mixed fluid regions. In these mixed regions, the relative velocity is a function of a droplet size, d_p. For the shear flow simulation a constant value of d_p was used, whereas for the three-bay model it was computed dynamically, using a Droplet Formation Model (DFM) [see Celik, Kandil and Badeau (2001)]. The SDC of fuel in water, ϕ, was advected using a scalar advection equation. At fuel/water interface points, defined as those points closest to, but exceeding $r = 0.50$, $\Delta\phi$ was generated as per (16). A FAVOR (Fractional Area/Volume Obstacle Representation) method is used to represent the geometry. The geometry was discretized with orthogonal, Cartesian single block meshes. The influence of turbulence was estimated using the standard $k-\varepsilon$ model for the shear flow and the RNG $k-\varepsilon$ model for the three-bay model simulations. The densities, ρ, of the fuel and water were assumed to be 850 kg/m^3 and 1000 kg/m^3, respectively. The dynamic viscosities, μ, were $2.0\times10^{-3}\ kg/(m\cdot sec)$ and $1.0\times10^{-3}\ kg/(m\cdot sec)$, respectively.

The computational geometry for the shear flow is shown in Figure 1. The water enters the lower right boundary, exiting at the lower left. The fuel enters at the upper left and exits at the upper right. The fuel/water interface occurs downstream of the splitter plate. More details of the actual experimental geometry are found in Wu and Katz (2001). Only the $0.8\ m/sec$ case has been used for validation. Droplet diameters $d_p = 0.2\ cm$ was used in the drift flux algorithm.

The three-bay model is an abbreviated version of three bays of a full-scale CFBT. Its purpose was to obtain effluent fuel concentration measurements in a tank with buoyant flow events similar to full-scale CFBT flows. The three-bay model is approximately 244 cm (96 in) long, 28 cm (11 in) wide, and 56 cm (22 in) high. The tank consists of three equal sized compartments, separated by baffles with rectangular "manholes." The manholes were sized and located such that the buoyant flow events through them replicated full-scale flows and, therefore, would generate fuel droplets under full-scale conditions. Initially, the tank was full of water with a 7.6 cm (3 in) layer of fuel at the top of each compartment. This initial fuel layer represents the residual fuel layer that is present in full-scale CFBTs at the beginning of refueling. The fuel enters the first compartment (shown at the right in Figure 10) vertically upward through the inlet pipe, and exits vertically upward through the exit pipe. The simulated fuel inflow rate was $2.2\ell/sec$.

Effluent fuel concentrations in the exit pipe of the three-bay model were obtained using an optical detection methodology. Digital images of a horizontal cross-section of the vertical exit pipe were taken from underneath the tank. The images were backlit from the top by a strobe light; the fuel droplets showed up as silhouettes. The droplets and effluent fuel concentrations were obtained from the images using automated droplet detection and sizing software. The smallest resolved droplet was approxi-

mately 100 μm in diameter.

Shear Flow Results

Figure 11 compares E computed from the droplet data, E predicted by the relationship (12) and E computed by the simulation. These results show that for small x ($< 15\ cm$), the quick increase to a peak is not simulated. However, the correct order of magnitude and slope after this peak is captured. A detailed study shows that for $x > 15\ cm$, the velocity shear compares very well with experiment but that the simulated fluid fraction gradients are too large. This results in Ri_α values that are too large, making the values of E too small in comparison to (12). Further investigations are underway in this area.

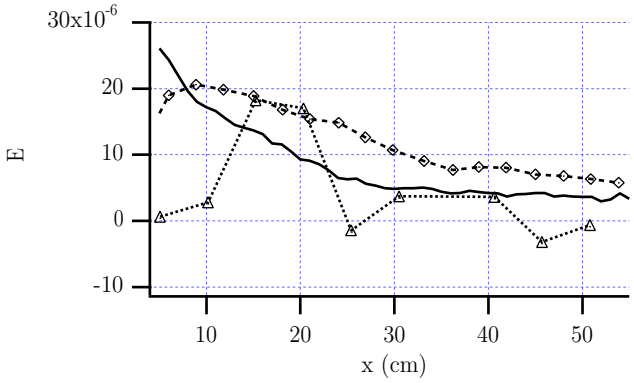

Figure 11. ENTRAINMENT MODEL RESULTS FOR SHEAR FLOW SIMULATION: E; △ : EXPERIMENT; ——— : SIMULATION; ◇ : EXPERIMENTAL CORRELATION EQN. (12).

Three Bay Model Results

Figure 12 shows a comparison of the effluent fuel concentrations from the experiment and from three simulations for the 2.2 ℓ/sec inflow rate case. The experimental data shown represents a 2 *sec* running average from four separate tests.

Results using correlation (12) (denoted by "Simulation 1") give values that may have some of the same trends but that are low by a factor of almost 10^2. It is believed that the primary reason for this discrepancy is that the correlation (12) was developed for a stably stratified shear flow and that it does not account for the droplet generation mechanisms in buoyant flow events. It has been observed in the three-bay model experiments as well as previous half-scale two-bay experiments that the buoyant flow events generate a large number of droplets and neutrally buoyant, water-filled oil-skinned "balloons" as shown in Figure 13, and close up, in Figure 14. In any case, it appears that a vertical velocity component at the interface either in jet itself, or

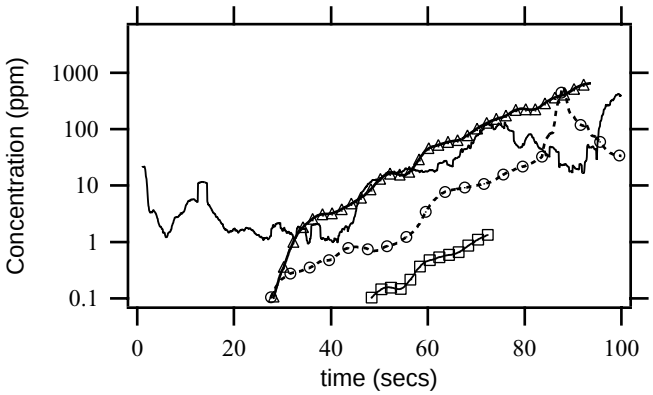

Figure 12. COMPARISON OF EFFLUENT FUEL CONCENTRATIONS FROM THREE-BAY MODEL EXPERIMENT AND PREDICTED BY COMPUTATIONAL SIMULATIONS: ——— : EXPERIMENT; □ : SIMULATION 1 (DEM BASED ON SHEAR FLOW); △ : SIMULATION 2 AND ○ : SIMULATION 3 (DEM INCLUDING EFFECTS OF BFES).

after it impacts the tank top (see computational results in Figure 15) may play a crucial role in the entrainment. In Simulation 2 $C_{e\alpha} = 1.0 \times 10^{-4}$. Figure 13 shows that this improves the overall level of effluent fuel concentrations, while damping out any of the features.

A correction method that incorporates the strong vertical velocities of a buoyant flow event may be to include the vertical velocity, w_k, in the convection velocity (15) as

$$U_c = \left[u_k^2 + v_k^2 + (bw_k)^2\right]^{1/2}. \tag{19}$$

where b is a user-specified constant. Results using (19) with $b = 100$ and $C_{e\alpha} = 1.0 \times 10^{-6}$ are shown Figure 12 labeled as "Simulation 3." Results show the correct features and levels are predicted but that there is a 15 *sec* lag.

SUMMARY

Correlations for the generation rate of the fuel concentration due to small fuel droplets at a stably stratified fuel/water interface have been proposed. The correlations are based on immiscible diesel fuel and water shear flow experimental droplet and velocity field data. The concentration generation rate includes droplets in the size range $0.7 - 1.5\ mm$. The correlations have been implemented in a two-fluid computational fluid dynamics code and have been run on two test cases. The first, the stably stratified shear flow, shows that the correlations can predict reasonable generation rates. The second, a three bay model with weak stably stratified shear flows and strong buoyant flows shows that the correlations underpredict the fuel concentration generation rate.

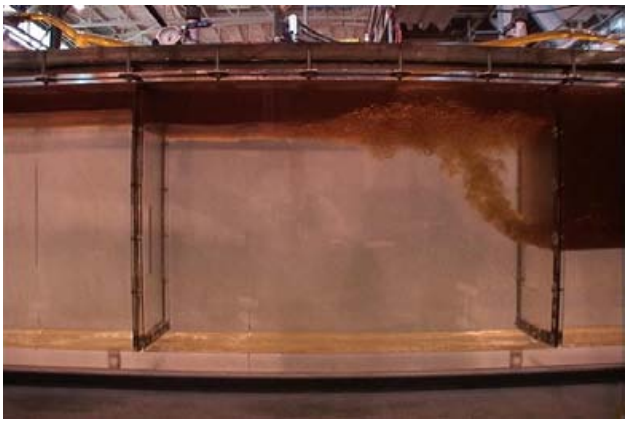

Figure 13. PHOTOGRAPH TAKEN DURING THREE-BAY MODEL TESTS ($2.2\ \ell/sec$) AT $t = 30\ sec$ SHOWING BUOYANT FLOW EVENT THROUGH THE FIRST MANHOLE.

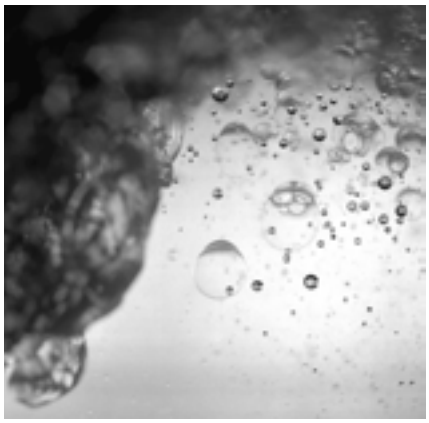

Figure 14. DROPLETS AND BALLOONS GENERATED BY A BUOYANT FLOW EVENT.

However, including the vertical interface velocity component in the entrainment rate formulation appears to capture some of the necessary physics.

ACKNOWLEDGEMENTS

This work was sponsored by the Naval Sea Systems Command (NAVSEA) Shipboard Pollution Abatement Project. The Research and Development Program Manager is Mr. Carl Adema (SEA 05MR) of the Research and Development Office. The Project Leader at the Naval Surface Warfare Center — Carderock Division (NSWCCD) is Mr. Stephan Verosto of the Pollution Prevention and Material Safety Branch (Code 632).

Those persons who made all the experiments at NSWCCD-SSES a success are due thanks: Mr. Lawrence Tomlinson of NSWCCD, Dr. John McGinn and Mr. Carl Schmid of GeoCenters, Inc., and Mr. Tom O' Connell of M. Rosenblatt and Son. Prof. Prof. Ismail Celik of West Virginia University is thanked for his guidance on computational and general fluid dynamics issues. Mrs. Allen Badeau, Andrew Burt, Sharif Kandil and Ms. Zeynep Cehreli are acknowledged for their assistance in development of the DFM and early versions of the DEM.

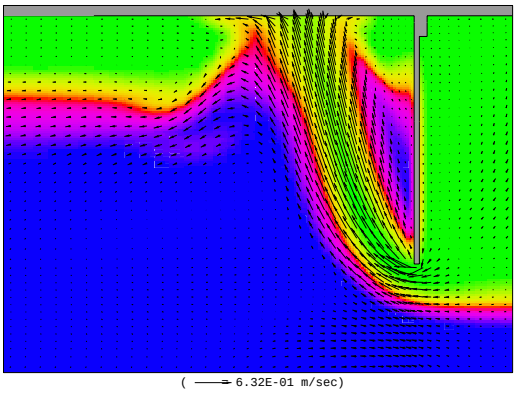

Figure 15. BUOYANT FLOW EVENT FROM SIMULATION.

REFERENCES

P. Chang, W. Wilson, S. Verosto, and P. Atsavapranee, Assessment of the refueling performance of ddg 51 compensated fuel/ballast tanks, in *ASNE Fleet Maintenance Symposium*, San Diego, CA, 2001, San Diego Section of the American Society of Naval Engineers.

H. J. Fernando, Annual Review of Fluid Mechanics **23**, 455 (1991).

P. Atsavapranee and M. Gharib, Journal of Fluid Mechanics **342**, 53 (1997).

X. Wu and J. Katz, On the flow structures and mixing phenomenon in a fuel-water stratified shear flow, in *3d ASME/JSME Joint Fluids Engineering Conference*, San Francisco, CA, 1999.

X. Wu and J. Katz, On the flow field near the interface and droplet characteristics in a fuel/water stratified shear flow, in *ASME 2000 Fluids Engineering Division Summer Meeting*, Boston, MA, 2000.

X. Wu and J. Katz, Mixing mechanisms and resulting droplet distributions in a fuel-water stratified shear flow, in *International Conference on Multiphase Flows*, New Orleans, LA, 2001.

I. Celik, S. Kandil, and A. Badeau, A computational study of mixing in a liquid jet impinging on an immiscible liquid layer, in *ASME 2001 Fluids Engineering Divsion Summer Meeting*, New Orleans, LA, 2001.